Isoelectronic Ga Substitution Effects on Antiferromagnetic Order in $CeRh(In_{1-x}Ga_x)_5$

Xin Li(李鑫)[1], Kai Wen Chen(陈锴文)[1], Cheng Yu Jiang(姜程予)[1], Jia Chen Jiao(焦嘉琛)[1], Mu Yuan Zou(邹牧远)[1], Oksana Zaharko[2], Bai Jiang Lv(吕柏江)[3], Guang-Ai Sun(孙光爱)[3], and Lei Shu(殳蕾)[1,4*]

[1]*State Key Laboratory of Surface Physics, Department of Physics, Fudan University, Shanghai 200438, China*
[2]*Paul Scherrer Institute Center for Neutron and Muon Sciences, 5232 Villigen PSI, Switzerland*
[3]*Key Laboratory of Neutron Physics and Institute of Nuclear Physics and Chemistry, China Academy of Engineering Physics, Mianyang 621999, China*
[4]*Shanghai Research Center for Quantum Sciences, Shanghai 201315, China*

(Received 23 January 2025; accepted manuscript online 16 June 2025)

In this work, Ga-doped $CeRhIn_5$ single crystals are grown by In/Ga flux method. Single-crystal X-ray diffraction, magnetic susceptibility, specific heat, and neutron diffraction measurements are utilized to characterize the sample quality and the antiferromagnetic transition temperature T_N. By substituting In with Ga, T_N is slightly decreased, but the antiferromagnetic transition peaks in magnetic susceptibility and specific heat measurements are obviously broadened by external field along c-axis. By comparing with Zn-doped $CeRhIn_5$, it can be concluded that T_N is dominated by electron density, and the stiffness of antiferromagnetic transition is obviously reduced by Ga substitution. The substitution effects of Ga are possibly caused by forming heterogeneous local structures, which avoids quantum critical point, superconductivity, and non-Fermi liquid states. Investigations on Ga-doped $CeRhIn_5$ help to comprehend the chemical substitution effects in $CeRhIn_5$, and the interaction between heterogeneous structure and long-range antiferromagnetic states.

DOI: 10.1088/0256-307X/42/8/080704 CSTR: 32039.14.0256-307X.42.8.080704

The competition between the Ruderman–Kittel–Kasuya–Yosida (RKKY) interaction and the Kondo effect induces quantum criticality in strongly correlated electron systems. The strengths of the RKKY and the Kondo interactions are determined by the exchange interactions between conduction electrons and f-electrons (c–f),[1] while c–f interactions can be tuned by external parameters such as pressure, magnetic field, or chemical substitution. In the vicinity of the quantum critical point (QCP), enhanced spin fluctuations are observed and unconventional superconductivity (SC) often emerges.[2–4] The evolution of the ground states with c–f interaction is described by the Doniach phase diagram.[1] $CeMIn_5$ (M = Co, Rh, Ir) family provides ideal examples for the study of this scenario.[5–7] For $CeCoIn_5$, the logarithmic divergences of specific heat divided by temperature $C(T)/T$ and the linear temperature dependence of resistivity in normal states, indicating a non-Fermion liquid (NFL) behavior,[5] suggest it locating near a QCP. SC is observed below $T_c = 2.3$ K with absence of magnetic order. External pressure tunes the ground state of $CeCoIn_5$ from the NFL state to heavy fermion metal state.[8,9] Interestingly, $CeIrIn_5$ locates between the antiferromagnetic (AFM) metal and QCP with coexistence of both magnetic order and SC.[7] Despite that unconventional SC and NFL behavior was observed near a hidden AFM QCP,[10] the situation of $CeRhIn_5$, however, is more complicated. A first-order transition from coexisting state to pure superconducting state with a critical pressure $P_c \sim 1.75$ GPa was observed.[6,11] $CeRhIn_5$ orders antiferromagnetically at Néel temperature $T_N = 3.8$ K under ambient pressure and zero magnetic field.[6] For $P < P_c$, AFM order induces a partially gapped Fermi surface, and SC is supposed to form on the residual density of states at Fermi level, from ambient pressure to $P = P_c$.[12] The superconducting states at $P > P_c$ and $P < P_c$ differ from each other, suggested by a threefold growth of $\Delta C/C(T_c)$[13] for $P > P_c$.

Except for external pressure, chemical doping is also applied to tune the ground states in $CeMIn_5$. The chemical substitution effects, however, are distinct from external pressure effects. For $CeCoIn_5$, hole doping, such as Cd,[14,15] Hg,[16] or Zn[17,18] doping induces AFM order; electron doping, e.g., Sn doping gradually tunes $CeCo(In_{1-x}Sn_x)_5$ to the NFL metal side.[19,20] Soft X-ray absorption spectroscopy,[20] de Haas–van Alphen effect,[21] and nuclear quadrupole resonance (NQR)[22,23] suggest

*Corresponding author. Email: leishu@fudan.edu.cn
© 2025 Chinese Physical Society and IOP Publishing Ltd. All rights, including for text and data mining, AI training, and similar technologies, are reserved.

that Sn substitution uniformly enhances the c–f hybridization, pushing 4f-electrons to more itinerant side; while Cd substitution would only change the electron states in vicinity, leaving the majority of the electronic states unchanged. A heterogeneous electron state with droplet-like local magnetism and non-magnetic superconducting matrix is then formed.[22,23] The correlation lengths of the magnetic droplets increase with doping, and finally form long-range magnetic orders.[15] Chemical doping has also been applied to tune the ground state of $CeRhIn_5$. However, electron doping like Sn only gradually suppresses T_N to 0 K for $CeRh(In_{0.93}Sn_{0.07})_5$, around which NFL behavior appears without any superconducting transition.[24–26] Hole doping like Hg or Zn initially suppresses and then raises T_N.[27–29] Neither a QCP nor a superconducting state appear at ambient pressure in Zn-, Hg-, and Cd-doped samples. It was suggested that heterogeneous electron states are also formed in hole-doped $CeRhIn_5$.[28] More experimental work is needed to investigate the inhomogeneous local structure, and its relation to exotic quantum states like QCP and unconventional SC.

In addition, both electron doping with Sn and hole doping with Hg, Zn and Cd change the electron state and lattice volume of $CeRhIn_5$. Sn doping expands the lattice parameters, while Zn doping shrinks it, resulting in opposite chemical pressure effects.[28] Further investigations are needed to distinguish the chemical substitution effects of electron density and chemical pressure changing. Both Ga and In belong to group ⅢA of the periodic table. Substituting In with Ga causes little change in the electron density. Therefore, the chemical substitution effects mainly come from the chemical pressure. However, isoelectronic Ga-doped $CeRhIn_5$ has not been reported yet. In this work, $CeRh(In_{1-x}Ga_x)_5$ single crystals are grown from In/Ga flux. Magnetic susceptibility, specific heat, and neutron diffraction are utilized to characterize the isoelectric Ga substitution effects on magnetic properties of $CeRhIn_5$.

Single crystals of $CeRh(In_{1-x}Ga_x)_5$ were grown from the In/Ga flux method. Ce rods (99.9%), Rh ingots (99.95%), In (99.99%), and Ga (99.99%) shots were weighed with molar ratio $1:1:20(1-y):20y$ ($y = 0$, 0.02, 0.04, 0.08, and 0.1 are nominal concentrations), and put into an alumina crucible. The crucible was encapsulated into an evacuated quartz tube. The assembly was heated to 1050 ℃. After staying there for 20 hours for homogeneity, it was steeply cooled to 750 ℃ in 2 hours at a rate of 150 ℃/h to avoid the formation of $CeIn_3$. The quartz tube was then slowly cooled to 450 ℃ with a rate of 2 ℃/h, after which the crystals and molten flux were separated by centrifugation. Thick plate-like crystals were obtained, with size gradually decreasing with increasing y. Extra In/Ga flux on the surface of crystals was further removed by diluted hydrochloric acid.

The elemental distributions on the single crystal surface were measured by energy dispersive X-ray Spectroscopy (EDS) using an Oxford X-Max^N 150 mm^2 detector (Oxford Instruments, Abingdon, UK). Magnetic susceptibilities were measured in a magnetic property measurement system (MPMS, Quantum Design) at temperatures between 1.8 K and 300 K, for external fields from 0.1 T to 7 T. Specific-heat measurements were performed on a physical property measurement system (PPMS, Quantum Design) down to 1.8 K for magnetic fields up to 9 T. Single-crystal X-ray diffraction (XRD) measurements were performed on a Bruker D8 advanced X-ray diffractometer. Powder XRD measurements were performed on a HaoYuan DX-2700BH X-ray diffractometer. Single crystal neutron diffraction down to 0.08 K was performed on the ZEBRA diffractometer with the incident neutron wavelength 1.383 Å, at Paul Scherrer Institute, Villigen, Switzerland.

Powder XRD pattern in Fig. 1(a) confirms the $HoCoGa_5$-type structure for nominal concentrations $0 \leq y \leq 0.1$. Bragg peaks from a small amount of indium are also observed. This is because the flux is hard to be totally removed, especially for small crystals with stepped surfaces. A typical single-crystal XRD pattern for the Ga-doped sample ($y = 0.04$) is shown in Fig. 1(b). The XRD pattern is similar to that of $CeMIn_5$,[30,31] indicating that the sample exhibits the same tetragonal structure as $CeMIn_5$. The inset in Fig. 1(b) shows the obtained single crystals. Their typical size changes from $\sim 6 \times 6 \times 0.5\,\text{mm}^3$ to $\sim 1 \times 1 \times 0.2\,\text{mm}^3$. The lattice constant c obtained by least-square fittings of the (0 0 L) peak positions is shown in the right axis of Fig. 1(c). The lattice constant c decreases steeply with y for $y < 0.04$, then more gradually for $0.04 \leq y \leq 0.08$. Further increasing y to 0.1 might cause a slight increase of c. Left axis of Fig. 1(c) shows the relation between actual concentrations x obtained from the EDS measurements and the nominal concentrations y. Unlike Zn doping, where the actual concentrations x are proportional to the nominal concentrations, the actual concentrations of Ga increase quickly with y and saturates when $y > 0.04$. The saturation of actual Ga concentration is also observed in Ga-doped Ce_2RhIn_8.[32] Note that the nominal concentration $y = 0.04$ and $y = 0.1$ corresponds to similar actual concentration $x = 0.038$ and 0.037, respectively. Thus the two samples would be noted as $x = 0.38$ ($y = 0.04$) and $x = 0.37$ ($y = 0.1$), respectively. The trends of lattice constants c and actual concentrations x as a function of y are consistent with each other. The concentration dependent of c, suggesting the success of doping, is shown in Fig. 1(d). Lattice constants decrease linearly with increasing x, with a slop $\mathrm{d}c(x)/\mathrm{d}x = -0.39(3)$ Å. Zn and Hg doping also decrease the lattice constants c and provide a chemical pressure.[28] Zn doping causes a decrease of 0.013 Å for actual $x = 0.023$,[28] comparable to the decrease of 0.012 Å for the Ga concentration $x = 0.024$. This indicates that Ga doping is as effective as Zn to provide a chemical pressure. Increasing the nominal concentration of Ga to $y = 0.12$ in the raw material leads to formation of Ce_2RhIn_8 phase, indicated by single crystal XRD [Fig. 5(a)]. This would be discussed below.

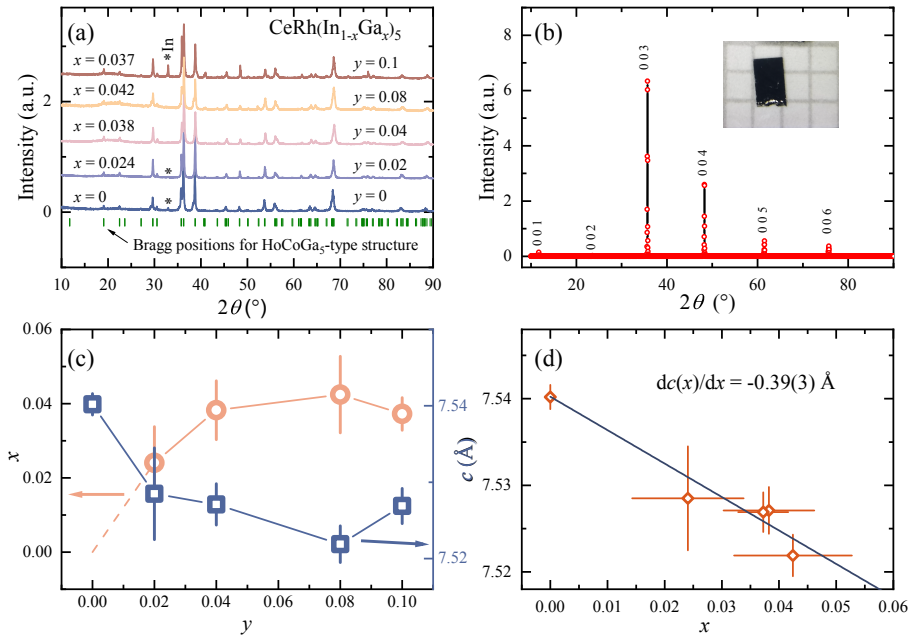

Fig. 1. (a) Powder XRD pattern for $CeRh(In_{1-x}Ga_x)_5$. All the Bragg peaks can be indexed by a $HoCoGa_5$-type structure along with a small amount of In flux. (b) Typical single crystal XRD pattern for Ga-doped $CeRhIn_5$ sample ($y = 0.04$), the inset shows the picture of the measured sample. (c) Left axis: actual concentrations x obtained from EDS as a function of nominal concentrations y; Right axis: lattice constants c as a function of nominal concentrations y, c is obtained from least square fitting of peak positions in single-crystal XRD pattern. (d) Relation between actual concentrations x and lattice constants c. The solid line shows a linear fit.

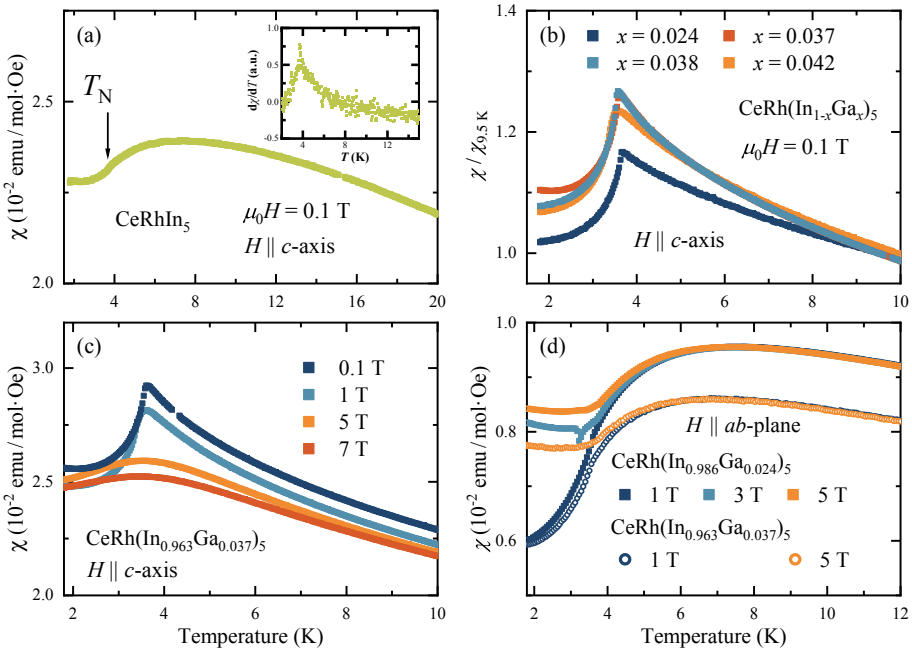

Fig. 2. Magnetic susceptibility of $CeRh(In_{1-x}Ga_x)_5$. (a) Temperature dependent magnetic susceptibility $\chi(T)$ for undoped $CeRhIn_5$ with applied field 0.1 T parallel to c-axis. A kink at 3.8 K represents the AFM transition temperature T_N. The derivation $d\chi(T)/dT$ shows a peak at T_N. (b) $\chi(T)/\chi(9.5\,K)$ with applied field 0.1 T parallel to c-axis for the $x = 0.024$, 0.037, 0.038, and 0.042 samples. A cusp at ~3.6 K can be observed instead a kink. (c) $\chi(T)$ for the $x = 0.037$ sample with various external fields parallel to the c-axis. The cusp feature at 0.1 T is broadened with higher fields. (d) $\chi(T)$ for the $x = 0.024$ (filled squares) and $x = 0.037$ (open circles) samples with various external fields parallel to the ab-plane.

Figure 2(a) shows the temperature dependence of magnetic susceptibility χ of $CeRhIn_5$ measured with the applied magnetic field $\mu_0 H = 0.1$ T along the c-axis. A kink at Neel temperature $T_N = 3.8$ K and a broad maximum near 7 K are observed. The kink indicates AFM transition, while the broad maximum is likely arising from short range order or spin fluctuations.[33] The broad maximum disappears and the kink changes to λ-like cusps,

even for the smallest concentration of gallium $x = 0.024$, as shown in Fig. 2(b). For $H \parallel c$-axis, λ-like cusps consistently appear when the magnetic moments are along the c-axis,[34–37] and the kinks are related to in-plane moment arrangements.[38,39] In the AFM phase of $CeRhIn_5$, the moments form a simple nearest-neighbor AFM order on a square lattice in the ab-plane with a twist along the c-axis.[40] The change of the magnetic response from kinks to cusps indicates that the arrangement of in-plane moments may be titled to exhibit a component along the c-axis. The characteristic temperatures of the cusps indicate T_N. T_N decreases slightly from 3.8 K for $x = 0$ to 3.56 K for $x = 0.042$. A Zn concentration $x = 0.017$ would decrease T_N to 3.1 K,[28] and a Hg concentration $x = 0.015$ would decrease T_N to 2.6 K.[27] Compared with $CeRh(In_{1-x}Zn_x)_5$ or $CeRh(In_{1-x}Hg_x)_5$ systems, T_N is less effected in $CeRh(In_{1-x}Ga_x)_5$. Figure 2(c) shows magnetic susceptibility for the $CeRh(In_{0.963}Ga_{0.037})_5$ sample with various external fields. The cusp moves to lower temperature, but remains its sharpness until the external field is 1 T. For external field of 5 T, the cusp becomes broad and the maximum moves to lower temperature. The broadening of the cusp indicates that the AFM transition is gradually suppressed by the external magnetic fields. In contrast to the case of $H \parallel c$, $\chi(T)$ curves for $H \parallel ab$-plane are similar to that of undoped $CeRhIn_5$. The $\chi(T)$ curve for the $x = 0.024$ sample with $\mu_0 H = 3$ T shows a drop at 3.4 K in Fig. 2(d), indicating a polarization of helical moments in the ab-plane, same as the case of $CeRhIn_5$.[33]

The λ-like peaks are observed in specific heat divided by temperature $C(T)/T$ for the $x = 0.038$ ($y = 0.04$) and $x = 0.037$ ($y = 0.1$) samples as shown in Fig. 3. The λ-like peak is similar to that of $CeRhIn_5$.[6] Characteristic temperatures for the peaks are consistent with T_N determined by magnetic susceptibility. Unlike to that of undoped $CeRhIn_5$, where λ-like feature persists with high magnetic fields applied parallel to the c-axis,[41,42] the λ-like cusp for both samples stays sharp over external field of 1 T, then is broadened significantly by the external field larger than 2 T. The broadening of AFM peak is also similar to that in Zn or Hg-doped $CeRhIn_5$.[28] The $C(T)/T$ peak heights for these samples at 0 T are 1.75 J/mol·K^2 and 1.43 J/mol·K^2, respectively, smaller than 2 J/mol·K^2 for $x = 0$.[6]

Figure 4 shows the single-crystal neutron diffraction scans for the $CeRh(In_{0.963}Ga_{0.037})_5$ sample. The (h h l) plane was set as the scattering plane, by using $\boldsymbol{Q}$ = (1 1 0) and (0 0 1) for sample alignment. Full width half maximum for the rocking curve around $\boldsymbol{Q}$ = (1 1 2) is 0.258(3)°, as shown in the inset of Fig. 4(a), indicating high quality of the sample. Previous neutron diffractions on $CeRhIn_5$ under pressure,[40,43–45] external magnetic fields,[46] or for doped $CeRhIn_5$[25,29] all contained magnetic peaks with $\boldsymbol{k}$-propagation vectors along (0.5 0.5 L). Magnetic $\boldsymbol{k}$-vector search was performed at 2 K and 0.08 K along the (0.5 0.5 L) direction. A L-scan from (0.5 0.5 0.2) to (0.5 0.5 1.2) at 2 K did not show any sign of a magnetic Bragg peak, as shown in Fig. 4(a). There are possible weak magnetic intensities near (0.5 0.5 0.39) when further cooling to 0.08 K, as shown in Fig. 4(c), the zoom-in plot of Fig. 4(a) near (0.5 0.5 0.4). Magnetic Bragg peaks at (0.5 0.5 0.61) and (0.5 0.5 1.39) are supposed to emerge as well, if there is an incommensurate magnetic $\boldsymbol{k}$-vector (0.5 0.5 0.39). However, no sign of magnetic Bragg peak can be observed near (0.5 0.5 0.61) and (0.5 0.5 1.39), as shown in Figs. 4(d) and Fig. 4(b), respectively. This may result from the extremely weak intensity. Our neutron diffraction data can not unambiguously claim a magnetic $\boldsymbol{k}$-vector near (0.5 0.5 0.39), further neutron diffraction experiments are needed. However, if it is the case, the staggered magnetic moment would be strongly reduced. The intensity of the magnetic Bragg peak normalized to intensity of $\boldsymbol{Q}$ = (1 1 2) nuclear peak is ∼100/6500 in $CeRhIn_5$,[44] corresponding to ordered magnetic moment $0.6\mu_B$. For the $CeRh(In_{0.963}Ga_{0.037})_5$ sample in this work, the normalized magnetic Bragg peak intensity is estimated to be smaller than 60/18000, almost 65/300 of the intensity in Ref. [44]. Therefore, the magnetic moment for the $CeRh(In_{0.963}Ga_{0.037})_5$ sample is roughly estimated to be smaller than $0.28\mu_B$, much smaller than the values in pressured[44] or doped $CeRhIn_5$.[25,29]

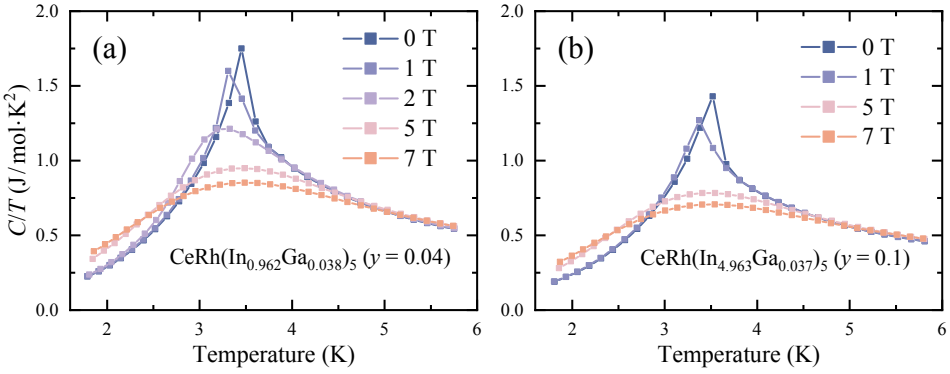

Fig. 3. Specific heat divided by temperature $C(T)/T$ for $CeRh(In_{1-x}Ga_x)_5$ with (a) $x = 0.038$ and (b) $x = 0.037$ samples. Two λ-like peaks corresponding to AFM transition emerge at 3.45 K and 3.52 K, respectively. Positions of peaks change to lower temperature when the external field increases to 1 T, and became broad maximums with higher fields.

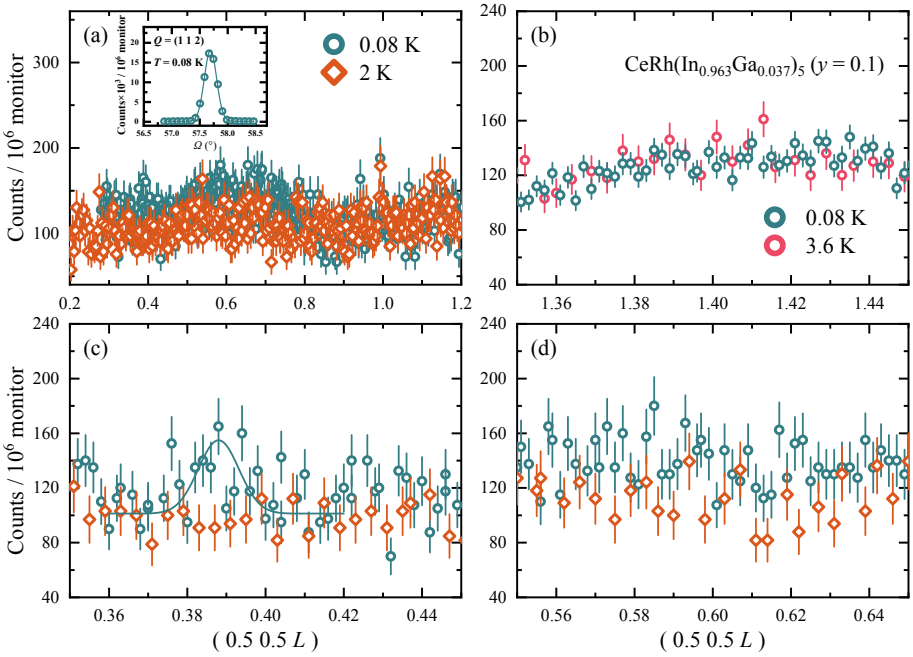

Fig. 4. Single crystal neutron diffraction for $CeRh(In_{5-x}Ga_x)_5$. (a) $\boldsymbol{Q}$-scan along (0.5 0.5 L) direction at 2 K and 0.08 K. Insert: Rocking curve for the nuclear Bragg peak with $\boldsymbol{Q}$ = (1 1 2) at 0.08 K. (b) $\boldsymbol{Q}$-scan near (0.5 0.5 1.4) at 3.6 K and 0.08 K. (c) Zoom-in plot of (a) near (0.5 0.5 0.4) at 2 K and 0.08 K. The solid line is added to guide the eyes. (d) Zoom-in plot of (a) near (0.5 0.5 0.6) at 2 K and 0.08 K.

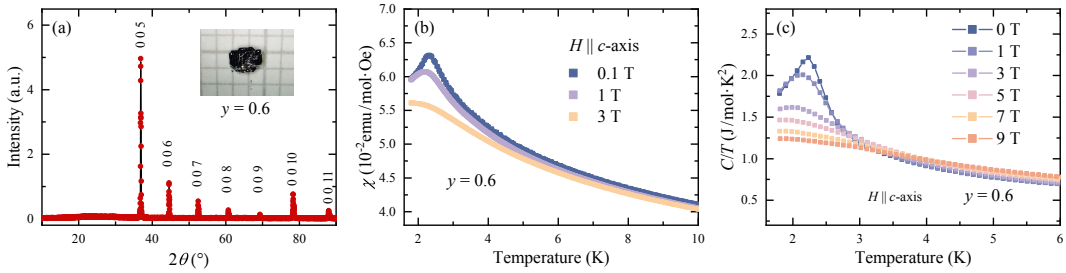

Fig. 5. Sample and characterization for the $y = 0.12$ sample. (a) Single-crystal XRD pattern of the $y = 0.12$ sample suggests a Ce_2RhIn_8-type structure. The insert shows a photo of the sample. (b) Magnetic susceptibility with $H \parallel c$-axis for the $y = 0.12$ sample. (c) Specific heat divided by temperature $C(T)/T$ with $H \parallel c$-axis for the $y = 0.12$ sample.

Further increasing nominal concentrations y to 0.12 results in the formation of Ce_2RhIn_8 phase, indicated by the single-crystal XRD pattern, obviously distinct from that of $CeRhIn_5$ phase, as shown in Fig. 5(a). The obtained lattice constant is $c = 12.205(1)$ Å, smaller than that of Ce_2RhIn_8.[47] The temperature dependence of χ shows a cusp at $T_N = 2.3$ K, but the cusp is broader than those for $CeRhIn_5$-type samples, as shown in Fig. 5(b). T_N is close to that of $Ce_2RhIn_{7.64}Ga_{0.36}$,[32] but is suppressed comparing to $T_N = 2.77$ K for Ce_2RhIn_8.[47] The AFM order is further evidenced by a cusp in $C(T)/T$, as shown in Fig. 5(c). The cusps in both $\chi(T)$ and $C(T)/T$ become broader with external field of 1 T along the c-axis. Similar to $CeRhIn_5$, AFM peaks of Ce_2RhIn_8 reported previously[48] remain sharp in external fields $H \parallel c$-axis to at least 8 T. Therefore, Ga doping assists external magnetic fields to suppress the AFM transition, in analogy to the case of $CeRh(In_{1-x}Ga_x)_5$.

The relation between T_N and Ga concentration x is displayed in Fig. 6. T_N is slightly suppressed to 3.56 K for the $x = 0.042$ sample, with the lattice constant c suppressed to 7.522(2) Å. For comparison, Zn doping with $x = 0.023$ simultaneously decreases the lattice constant c to 7.527 Å and suppresses T_N to 3 K.[28] It should be noted that Zn doping simultaneously introduces both a hole doping and a chemical pressure effect, while the dominant chemical substitution effects for Ga is from chemical pressure. Therefore, it can be concluded that T_N is more sensitive to electron density rather than to lattice shrinking. This is consistent with the scenario that chemical pressure causes only a change of the local structure, leaving the electronic structure and correlation strength of the AFM matrix nearly unchanged. However, for Ga-doped Ce_2RhIn_8, T_N is suppressed obviously from 2.77 K to 2.3 K. This may arise from that Ga doping changes the crystalline electric field ground-state wave function and increases the energies of the first and second excited states,[32] despite that the electron density is unchanged.

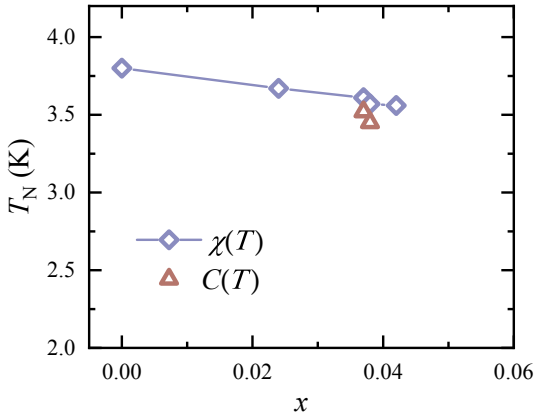

Fig. 6. T_N observed in magnetic susceptibility (open diamonds) and specific heat (open triangles) as a function of Ga concentration x for $CeRhIn(In_{1-x}Ga_x)_5$.

Despite that T_N changes little with Ga doping, the stiffness of the AFM transition against $H \parallel c$-axis is significantly reduced by Ga doping. The λ-like peaks in magnetic susceptibility and specific heat of $CeRhIn_5$ persist for magnetic fields up to 30 T.[41,42] Even for pressured $CeRhIn_5$, the AFM peaks are also sharp against external fields up to at least 6 T.[49] For both Zn and Ga doping, however, broaden of AFM peaks in specific heat is observed. Therefore, the broaden of AFM peaks is due to chemical pressure effect. Formation of a heterogeneous electronic state by local chemical pressure may influence the AFM transition with external fields $H \parallel c$-axis. In the case of $CeCoIn_5$, local magnetic droplets around dopants were previously revealed by NQR[22,50] and μSR experiments.[51] The correlation length of the droplets increases with increasing of Cd concentration, and eventually forms a long range AFM order in the non-magnetic matrix of $CeCoIn_5$.[15] For doped $CeRhIn_5$, however, the ground state of $CeRhIn_5$ is an AFM metal,[6] different from a non-magnetic superconducting state in $CeCoIn_5$.[5] Local chemical pressure provided by Zn or Ga dopants would more probably tune a non-magnetic local structure according to Doniach phase diagram. A possible non-magnetic local structure is indicated by the decreasing of $C(T)/T$ peak height with Ga or Zn doping. The correlation strength of the Ce^{3+} spins is insensitive to the non-magnetic local structure, and thus insensitive to Ga doping at zero or low external fields. Nevertheless, the non-magnetic droplets should be polarized and strongly compete with the AFM ground state of the matrix. This scenario explains the reduction of stiffness against external fields, while T_N keeps nearly unchanged with Ga doping at zero or low external fields. The chemical pressure effects provided by doping is different from hydrostatic external pressure effects. Formation of a heterogeneous electronic state avoids QCP, SC, and NFL states, which are seldom observed in hole-doped $CeRhIn_5$.

Both hole doping (Zn, Hg)[28] and Ga doping change the kink behavior into a cusp behavior in $\chi(T)$. This was also ascribed to the formation of magnetic local structure.[28] For $\chi(T)$ curves corresponding to an AFM transition with $H \parallel c$-axis, a kink is always observed when magnetic moments are aligned in the ab-plane (such as the case of $BaFe_2As_2$[38,39]); while a cusp is observed if there are components of magnetic moments along c-axis (such as the case of USb_2[34,35] and $PrCu_2Si_2$[36,37]). A more plausible explanation is that the dopants cant the in-plane moments of Ce^{3+},[40] and induce a magnetic component along the c-axis. Further neutron diffraction or μSR investigations are needed to explore the magnetic structure and the heterogeneous local structure in $CeRh(In_{1-x}Ga_x)_5$.

In summary, isoelectronic Ga-doped $CeRhIn_5$ single crystals are grown and characterized by single crystal XRD, magnetization, specific heat, and neutron diffraction methods. T_N, indicated by λ-like cusps in $\chi(T)$ and $C(T)/T$, is slightly suppressed by Ga doping. Meanwhile, the AFM transition cusps in $\chi(T)$ and $C(T)/T$ are broadened with applied fields $H \parallel c$-axis. By comparing with the results of hole-doped $CeRh(In_{1-x}Zn_x)_5$, it can be concluded that the suppression of T_N is due to the change of electron density. Despite T_N is nearly unaffected, the stiffness of AFM transition is obviously reduced. This is possibly due to the formation of a non-magnetic local structure around Ga dopants. Formation of non-magnetic local structures prevents $CeRh(In_{1-x}Ga_x)_5$ from QCP, SC and NFL states. These results help to distinguish effects of chemical pressure and electron density variation on T_N, and to comprehend the interaction between heterogeneous structure and long range AFM states.

Acknowledgements. This work is based on experiments performed at the Swiss Spallation Neutron Source (SINQ), Paul Scherrer Institute, Villigen, Switzerland. This work was supported by the National Key Research and Development Program of China (Grant No. 2022YFA1402203), the National Natural Science Foundations of China (Grant Nos. 12174065 and 12104424), and the Shanghai Municipal Science and Technology (Grant No. 2019SHZDZX01).

References

[1] Doniach S 1977 *Physica B* **91** 231
[2] Pfleiderer C 2009 *Rev. Mod. Phys.* **81** 1551
[3] Stewart G R 2001 *Rev. Mod. Phys.* **73** 797
[4] Maple M B, Baumbach R E, Butch N P, Hamlin J J, and Janoschek M 2010 *J. Low. Temp. Phys.* **161** 4
[5] Petrovic C, Pagliuso P G, Hundley M F, Movshovich R, Sarrao J L, Thompson J D, Fisk Z, and Monthoux P 2001 *J. Phys.: Condens. Matter* **13** L337
[6] Hegger H, Petrovic C, Moshopoulou E G, Hundley M F, Sarrao J L, Fisk Z, and Thompson J D 2000 *Phys. Rev. Lett.* **84** 4986
[7] Petrovic C, Movshovich R, Jaime M, Pagliuso P G, Hundley M F, Sarrao J L, Fisk Z, and Thompson J D 2001 *Europhys. Lett.* **53** 354
[8] Sparn G, Borth R, Lengyel E, Pagliuso P G, Sarrao J L, Steglich F, and Thompson J D 2001 *Physica B* **319** 262
[9] Knebel G, Measson M A, Salce B, Aoki D, Braithwaite D, Brison J P, and Flouquet J 2004 *J. Phys.: Condens. Matter.* **16** 8905
[10] Park T, Ronning F, Yuan H Q, Salamon M B, Movshovich R, Sarrao J L, and Thompson J D 2006 *Nature* **440** 65
[11] Park T and Thompson J D 2009 *New J. Phys.* **11** 055062

[12] Chen G F, Matsubayashi K, Ban S, Deguchi K, and Sato N K 2006 *Phys. Rev. Lett.* **97** 017005

[13] Paglione J, Ho P C, Maple M B, Tanatar M A, Taillefer L, Lee Y, and Petrovic C 2008 *Phys. Rev. B* **77** 100505

[14] Pham L D, Park T, Maquilon S, Thompson J D, and Fisk Z 2006 *Phys. Rev. Lett.* **97** 056404

[15] Nicklas M, Stockert O, Park T, Habicht K, Kiefer K, Pham L D, Thompson J D, Fisk Z, and Steglich F 2007 *Phys. Rev. B* **76** 052401

[16] Booth C H, Bauer E D, Bianchi A D, Ronning F, Thompson J D, Sarrao J L, Cho J Y, Chan J Y, Capan C, and Fisk Z 2009 *Phys. Rev. B* **79** 144519

[17] Yokoyama M, Mashiko H, Otaka R, Sakon Y, Fujimura K, Tenya K, Kondo A, Kindo K, Ikeda Y, Yoshizawa H, Shimizu Y, Kono Y, and Sakakibara T 2015 *Phys. Rev. B* **92** 184509

[18] Yokoyama M, Fujimura K, Ishikawa S, Kimura M, Hasegawa T, Kawasaki I, Tenya K, Kono Y, and Sakakibara T 2014 *J. Phys. Soc. Jpn.* **83** 033706

[19] Bauera E D, Moreno N O, Mixson D J, Sarrao J L, Thompson J D, Hundley M F, Movshovich R, and Pagliuso P G 2005 *Phys. B* **35** 359

[20] Chen K, Strigari F, Sundermann M, Hu Z, Fisk Z, Bauer E D, Rosa P F S, Sarrao J L, Thompson J D, Herrero-Martin J, Pellegrin E, Betto D, Kummer K, Tanaka A, Wirth S, and Severing A 2018 *Phys. Rev. B* **97** 045134

[21] Capan C, Jo Y J, Balicas. L, Goodrich R G, DiTusa J F, Vekhter I, Murphy T P, Bianchi A D, Pham L D, Cho J Y, Chan J Y, Young D P, and Fisk Z 2010 *Phys. Rev. B* **82** 035112

[22] Sakai H, Ronning F, Zhu J X, Wakeham N, Yasuoka H, Tokunaga Y, Kambe S, Bauer E D, and Thompson J D 2015 *Phys. Rev. B* **92** 121105

[23] Seo S, Lu X, Zhu J X, Urbano R R, Curro N, Bauer E D, Sidorov V A, Pham L D, Park T, Fisk Z, and Thompson J D 2014 *Nat. Phys.* **10** 120

[24] Bauer E D, Mixson D, Ronning F, Hur N, Movshovich R, Thompson J D, Sarrao J L, Hundley M F, Tobash P H, and Bobev S 2006 *Phys. B* **378** 142

[25] Knebel G, Buhot J, Aoki D, Lapertot G, Raymond S, Ressouche E, and Flouquet J 2011 *J. Phys. Soc. Jpn.* **80** SA001

[26] Raymond S, Buhot J, Ressouche E, Bourdarot F, Knebel G, and Lapertot G 2014 *Phys. Rev. B* **90** 014423

[27] Bauer E D, Ronning F, Maquilon S, Pham L D, Thompson J D, and Fisk Z 2008 *Phys. B* **403** 1135

[28] Park T B, Shin S, Lee S, Seo S, Jang H, Kim J, Lee H, Wang H, Lee H, and Park T 2020 *Phys. Rev. Mater.* **4** 084801

[29] Bao W, Gasparovic Y C, Lynn J W, Ronning F, Bauer E D, Thompson J D, and Fisk Z 2009 *Phys. Rev. B* **79** 092415

[30] Jia X W, Liu Y, Yu L, He J F, Zhao L, Zhang W T, Liu H Y, Liu G D, He S L, Zhang J, Lu W, Wu Y, Dong X L, Sun L L, Wang G L, Zhu Y, Wang X Y, Peng Q J, Wang Z M, Zhang S J, Yang F, Xu Z Y, Chen C T, and Zhou X J 2011 *Chin. Phys. Lett.* **28** 057401

[31] Park W K, Greene L H, Sarrao J L, and Thompson J D 2007 *Phys. C* **460** 206

[32] Caffer A M, Ajeesh M O, Carvalho M H, Mercena S G, Freitas G S, Pizzi H B, Passos D S, Adriano C, Bauer E D, Thompson J D, Ronning F, Thomas S M, Rosa P F S, and Pagliuso P G 2024 *Phys. Rev. B* **110** 205105

[33] Takeuchi T, Inoue T, Sugiyama K, Aoki D, Tokiwa Y, Haga Y, Kindo K, and Onuki Y 2001 *J. Phys. Soc. Jpn.* **70** 877

[34] Wawryk R 2006 *Philos. Mag.* **86** 1775

[35] Leciejewicz J, Troc R, Murasik A, and Zygmunt A 1967 *Phys. Stat. Sol.* **22** 517

[36] Ivanov V, Kolenda M, Leciejewicz J, Stfisser N, and Szytuta A 1996 *J. Alloys. Compd.* **234** L4

[37] Dung N D, Ota Y, Sugiyama K, Matsuda T D, Haga Y, Kindo K, Hagiwara M, Takeuchi T, Settai R, and Onuki Y 2009 *J. Phys. Soc. Jpn.* **78** 024712

[38] Rotter M, Tegel M, Johrendt D, Schellenberg I, Hermes W, and Pottgen R 2008 *Phys. Rev. B* **78** 020503

[39] Huang Q, Qiu Y, Bao W, Green M A, Lynn J W, Gasparovic Y C, Wu T, Wu G, and Chen X H 2008 *Phys. Rev. Lett.* **101** 257003

[40] Bao W, Pagliuso P G, Sarrao J L, Thompson J D, Fisk Z, Lynn J W, and Erwin R W 2000 *Phys. Rev. B* **62** R14621

[41] Mishra S, Demuer A, Aoki D, and Sheikin I 2021 *Phys. Rev. B* **103** 045110

[42] Jiao L, Smidman M, Kohama Y, Wang Z S, Graf D, Weng Z F, Zhang Y J, Matsuo A, Bauer E D, Lee H, Kirchner S, Singleton J, Kindo K, Wosnitza J, Steglich F, Thompson J D, and Yuan H Q 2019 *Phys. Rev. B* **99** 045127

[43] Majumdar S, Balakrishnan G, Lees M R, Paul D M, and McIntyre G J 2002 *Phys. Rev. B* **66** 212502

[44] Llobet A, Gardner J S, Moshopoulou E G, Mignot J M, Nicklas M, Bao W, Moreno N O, Pagliuso P G, Goncharenko I N, Sarrao J L, and Thompson J D 2004 *Phys. Rev. B* **69** 024403

[45] Aso N, Ishii K, Yoshizawa H, Fujiwara T, Uwatoko Y, Chen G F, Sato N K, and Miyake K 2009 *J. Phys. Soc. Jpn.* **78** 073703

[46] Raymond S, Ressouche E, Knebel G, Aoki D, and Flouquet J 2007 *J. Phys.: Condens. Matter* **19** 242204

[47] Nicklas M, Sidorov V A, Borges H A, Pagliuso P G, Petrovic C, Fisk Z, Sarrao J L, and Thompson J D 2003 *Phys. Rev. B* **67** 020506

[48] Ueda T, Shishido H, Hashimoto S, Okubo T, Yamada M, Inada Y, Settai R, Harima H, Galatanu A, Yamamoto E, Nakamura N, Sugiyama K, Takeuchi T, Kindo K, Namiki T, Aoki Y, Sato H, and Onuki Y 2004 *J. Phys. Soc. Jpn.* **73** 649

[49] Knebel G, Aoki D, Braithwaite D, Salce B, and Flouquet J 2006 *Phys. Rev. B* **74** 020501

[50] Urbano R R, Young B L, Curro N J, Thompson J D, Pham L D, and Fisk Z 2007 *Phys. Rev. Lett.* **99** 146402

[51] Howald L, Stilp E, Reotier P D, Yaouanc A, Raymond S, Piamonteze C, Lapertot G, Baines C, and Keller H 2015 *Sci. Rep.* **5** 12528